HHS Public Access

Author manuscript

ACS Macro Lett. Author manuscript; available in PMC 2023 April 19.

Published in final edited form as:

ACS Macro Lett. 2022 April 19; 11(4): 460–467. doi:10.1021/acsmacrolett.2c00053.

Synthesis and Micellization of Bottlebrush Poloxamers

Joseph F. Hassler[1], **Nicholas J. Van Zee**[2], **Adelyn A. Crabtree**[1], **Frank S. Bates**[1,*], **Benjamin J. Hackel**[1,*], **Timothy P. Lodge**[1,2,*]

[1]Department of Chemical Engineering and Materials Science, University of Minnesota, Minneapolis, MN 55455

[2]Department of Chemistry, University of Minnesota, Minneapolis, MN 55455

Abstract

Bottlebrush polymers are characterized by an expansive parameter space, including graft length and spacing along the backbone, and these features impact various structural and physical properties such as molecular diffusion and bulk viscosity. In this work, we report a synthetic strategy for making grafted block polymers with poly(propylene oxide) and poly(ethylene oxide) side chains, bottlebrush analogues of poloxamers. Combined anionic and sequential ring-opening metathesis polymerization yielded low dispersity polymers, at full conversion of the macromonomers, with control over graft length, graft end-groups, and overall molecular weight. A set of bottlebrush poloxamers (BBPs), with identical graft lengths and composition, was synthesized over a range of molecular weights. Dynamic light scattering and transmission electron microscopy were used to characterize micelle formation in aqueous buffer. The critical micelle concentration scales exponentially with overall molecular weight for both linear and bottlebrush poloxamers; however, the bottlebrush architecture shifts micelle formation to a much higher concentration at comparable molecular weight. Consequently, BBPs can exist in solution as unimers at significantly higher molecular weights and concentrations than the linear analogues.

Graphical Abstract

[*]Authors for correspondence: bates001@umn.edu, hackel@umn.edu, lodge@umn.edu.

Supporting Information:

Materials, methods, anionic and post polymerization hydrogenation characterization via ^{1}H NMR (Fig. S1), SEC characterization of a ROMP polymerization with the alkene impurity (Fig. S2), additional MALDI characterization of PPO macromonomer (Fig. S3), 1H and MALDI characterization of PEO macromonomer (Fig. S4), polymer characterization data (Figs. S5–S7), additional cryo-TEM micrographs (Figs. S8–S9), modelling of DLS data (Fig. S10), DLS correlation functions (S11–13), multi-angle DLS data (Fig. S14), micelle stability assessment (Fig. S15), a model of micelle dimensions (Fig. S16), and SEC characterization of PEO20k linear control used for DLS experiments (Fig. S17) are shown in the supporting information.

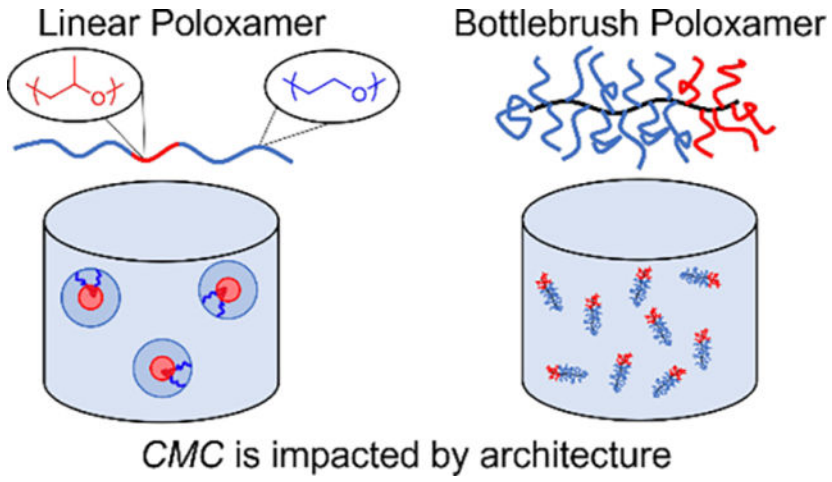

Block polymer amphiphiles in aqueous environments assemble into diverse micelle and vesicle morphologies,[1,2] with applications in numerous fields including pharmaceutical delivery[3,4] and as nanoreactors.[5] Additionally, single chains or unimers interact with phospholipid bilayers in therapeutically relevant ways, ranging from membrane solubilization to stabilization.[6–12]

Poloxamers are a specific class of linear block polymer amphiphile of poly(ethylene oxide) (PEO) and poly(propylene oxide) (PPO) that are commercially available (e.g., Pluronics®), biocompatible, and have demonstrated efficacy as cell membrane stabilizing agents against many types of stresses.[11,13–15,16] A range of prior studies have focused on the mechanisms of poloxamer-lipid interactions; however, a complete picture of the stabilization mechanism is still lacking.[17,18,27–30,19–26] Amphiphilic bottlebrush polymers have potential as a tool to yield additional mechanistic insights, through architectural variation. Bottlebrush polymers have multiple parameters to tune (e.g., backbone length, graft length, graft spacing) and aspects of the relationships among these parameters and molecular properties such as segmental dynamics,[31–33] molecular shape,[34] and ability to share space,[35–38] are understood. Thus, a synthetic platform that enables bottlebrush block polymers with PEO and PPO side chains, “bottlebrush poloxamers (BBPs),” with control over molecular parameters could enable pursuit of many structure-function hypotheses to elucidate mechanisms of polymer-lipid membrane interactions.

Synthesis of BBPs is challenging. Controlled radical polymerization can produce grafted PPO polymers; however, these methods require low monomer conversion or low grafting density to maintain modest dispersities.[4,39–43] In this work, we disclose a synthetic route to BBPs that circumvents these challenges and gives more control over parameters such as graft length and graft density. We then examine the micellization behavior of a set of BBPs to understand the relationship between the apparent critical micellization concentration (CMC_a) and the total molecular weight. The resulting scaling relationship provides a comparison of the thermodynamic drive towards micellization between the bottlebrush and the chemically analogous linear architectures.

Our synthetic route is shown in Scheme 1. Living anionic polymerization followed by chain end modification was used to make norbornene (NB)-functionalized macromonomers (MMs), which were then polymerized via ring opening metathesis polymerization (ROMP). ROMP has successfully been combined with living polymerization strategies such as anionic, RAFT, and ATRP and is compatible with PEO.[44–47] This strategy has several advantages. First, anionic polymerization can yield low dispersity PEO and PPO polymers of a targeted molecular weight with well-defined α-chain ends.[11,48,49] Second, ROMP of NB macromonomers reaches >99% conversion within minutes. Third, ROMP avoids chain transfer/coupling side reactions that are often observed during radical polymerization, to which PPO macromonomers are vulnerable due to the abstractable proton on the tertiary carbon site of every repeat unit.[50] Together, these advantages enable high-throughput synthesis of high molecular weight, high grafting density, low dispersity BBPs with control over graft length and graft end group. The nomenclature adopted throughout is BB-$E_{q,p}$-*b*-BB-$P_{n,m}$ where "BB" indicates bottlebrush, "E" and "P" indicate PEO and PPO respectively, and the subscripts are number average degrees of polymerization in reference to Scheme 1.

The black trace in Fig. 1 shows matrix-assisted laser desorption/ ionization mass spectrometry (MALDI) data of the product PPO from anionic polymerization. Notably, there are two populations with peak spacings of 58 g/mol, indicating both are PPO. The more intense family of peaks is the desired product with a *tert*-butyl α-chain end and an alcohol ω-chain end (*t*-PPO-OH). The family labelled with blue squares is an impurity with an alkene α-chain end, arising from deprotonation of PPO methyl groups during polymerization.[51] This assessment is confirmed by ^{1}H nuclear magnetic resonance (NMR) spectroscopy, as shown in Fig. S1. We employed established methods to limit this side reaction using 18-crown-6 ether,[49,51] but roughly 7 mol% (from NMR) of the chains have this impurity. We expected this alkene impurity to be susceptible to cross-metathesis during ROMP, leading to high dispersity polymers with limited control over molecular weight, Fig. S2.[52] Thus, we performed a post-polymerization hydrogenation to eliminate this alkene impurity. The MALDI data in Fig. 1 show a 2 g/mol increase in molecular weight for each of the peaks identified in the alkene chain end population, blue squares to green circles, which indicates that this chain end modification was successful without changing the molecular weight distribution.

The final step of MM preparation was to convert the ω-alcohol to a NB-ester through a modified protocol for the PPO chemistry.[3,53] Fig. 2a shows a close-up of the MALDI spectrum to highlight the peak shifting after chain end modification; the full spectrum can be found in Fig. S3a. The blue triangle population, present as the majority in the starting material (black spectrum) and a minority in the product (blue spectrum), is *t*-PPO-OH. After esterification, this population shifts by +4 g/mol in *m/z* (yellow stars), indicating successful addition of a NB unit. Note that adjacent peaks do not have the same degree of polymerization, thus the expected peak shift after an end group modification is the difference in molecular weight of the end groups minus an integer multiple of the repeat unit molecular weight. A similar shift, +6 g/mol, occurs between the blue square and yellow circle populations, which correspond to the alkene-PPO-OH and alkane-PPO-NB, respectively. Note the black trace is from the material prior to hydrogenation while the blue trace is post-hydrogenation and esterification. Fig. S3c shows size exclusion

chromatography (SEC) traces of the PPO post anionic polymerization and the functionalized MM, and the molecular weight distributions are identical. ^{1}H NMR spectroscopy was used to assess the purity of the resulting polymer and to corroborate successful chain end modification. The peak shape and integration of the alkene multiplet at 6.09–6.24 ppm (Fig. 2B) suggests that 95 mol% of the NB is on a polymer chain end.[54] Excess NB-carboxylic acid was needed to achieve high conversion and was difficult to remove due to its similar hydrophobicity to PPO and the small molecular weight of the PPO. We deemed this level of purity to be acceptable, but there will be some incorporation of NB-carboxylic acid in the polymer backbone. When accounting for the small molecule (~5 mol%) and the alkane ω-end group (~7 mol%) impurities in the analysis of the integral values of the NB peaks (6, 7, 8), which were referenced to the *t*-butyl peak (1), we conclude that quantitative conversion of alcohol to NB at the ω-end groups was achieved. A similar protocol was used to synthesize a NB-functionalized MM from a commercial methyl ether PEO (M_n = 1970 g/mol, $Đ$ = 1.04). MALDI and ^{1}H NMR characterization are shown in Fig. S4.

After synthesis of MMs, sequential ROMP afforded a grafted polynorbornene diblock polymer, where one block has PEO side chains and the other PPO sidechains. To our knowledge, this is the first report of a bottlebrush PEO-*b*-PPO polymer. The representative SEC traces in Fig. 3 show that both the PPO block and the diblock have narrow dispersities, achieve the target molecular weight, and shift systematically to shorter retention times for higher M_n. The ^{1}H NMR spectrum in Figure S6b shows complete conversion of the monomeric NB alkene peaks to backbone alkene peaks, confirming that the reaction achieved full conversion of monomer. To our knowledge, this is the first report of a grafted PPO polymer where the macromonomer was fully consumed, making synthesis of multi-blocks possible. SEC traces and ^{1}H NMR spectra for all polymers discussed in this report are shown in Figs. S5–S7.

To understand the micellization behavior of these BBPs, we synthesized three polymers with constant side chain lengths and similar compositions (70–80 wt% PEO), with total molecular weights ranging from 26 kDa to 394 kDa. All materials had narrow molecular weight distributions ($Đ$ < 1.15), and the characterization data are summarized in Table 1. Micelle solutions were prepared via direct dissolution in aqueous buffer and were equilibrated at 37 °C for at least 24 hours. The CMC_a and hydrodynamic radii (R_h) were determined via dynamic light scattering (DLS). DLS measures the diffusive relaxation of concentration fluctuations in dilute solution, which yields the particle size distribution by analyzing the correlation function via cumulant analysis or inverse Laplace techniques such as regularized positive exponential sum.[55–58]

To estimate the CMC_a, we analyzed the excess scattering intensity ($I_{ex} = I - I_{solvent}$) as a function of polymer concentration.[60,61] Because I_{ex} scales with the product of the number of scatterers and the size of the scatters, the concentration at which I_{ex} increases relative to the control (linear PEO homopolymer with M_n = 20 kDa) indicates aggregation (Fig. 4a). To ensure that the aggregates are micelles, we performed cryo-transmission electron microscopy (TEM) on the smallest and largest BBPs. A representative micrograph of the largest polymer is shown in Fig. 4b, which clearly demonstrates a core-corona structure.

Micrographs of the smallest polymer clearly show a core, although the corona block is too short to be observed. Additional micrographs are shown in Figs. S8–9.

On qualitative inspection of Fig. 4a, as M_n increases, the CMC_a decreases. Quantitative analysis is challenging because micellization is not a phase transition; therefore, a precise CMC_a is difficult to extract and is sensitive to the method employed.[62, 63] A representative CMC_a was taken as the intersection of two logarithmic fits: one at low polymer concentrations, and one at high polymer concentrations, representing the free chain and micelle regimes, respectively. The error is estimated as the difference in the CMC_a when the number of data points in the micelle regime is increased by 1. To ensure these CMC_a estimates are representative, we also fit the DLS data to a closed association model,[62,64] which includes the CMC_a as a fitting parameter (Fig. S10). Consistent trends were observed with both methods.

The relationship between M_n and CMC_a for 80 wt% PEO linear poloxamers[59] and 72–80 wt% PEO BBPs are shown in Fig. 4c. The free energy of a micelle is the sum of the core-corona interfacial energy, the energy of chain deformation, and the entropy of mixing between solvent and corona units. The closed association model asserts that above the CMC_a there is an equilibrium between unimers ([unimers] = CMC_a) and micelles of a constant size. Minimization of the total free energy of the system (micelles, unimers, and solvent) yields an exponential scaling between the CMC_a and M_n.[60,62,65,66] Therefore, the data are fit to an exponential form as shown in Eq. 1.

$$CMC_a = A \times e^{-\alpha \times M_n} \quad (1)$$

Strikingly, the coefficient in the exponent of the fit (slope in Fig. 4c) is two orders of magnitude smaller in the bottlebrush case than in the linear case. Because $\alpha \sim \chi$, the Flory-Huggins interaction parameter, the reduced scaling coefficient suggests a decreased degree of solvent-core incompatibility, and therefore reduced thermodynamic driving force for micellization, in BBPs than in linear poloxamers. One explanation for this is that the PPO units near the hydrophobic NB backbone are relatively dehydrated in the unimer state. Thus, some of the entropic gain in the solvent upon dehydrating PPO in going from unimer to micelle is lost. Additionally, a BBP with $M_n \sim 400$ kDa has a comparable CMC_a to a linear poloxamer with $M_n \sim 14$ kDa, which is consistent with a recent molecular dynamics result.[67] This finding is of practical significance because in BBPs the CMC_a is less sensitive to molecular weight, enabling synthesis of vastly higher M_n materials that will exist as unimers in aqueous solutions.

This reduction of α for BBPs compared to linear poloxamers cannot be explained by the hydrophobic backbone. If the added hydrophobicity of the backbone were a significant contributor to micellization, we would observe the opposite effect, namely the BBPs would form micelles at lower concentrations compared to linear poloxamers due to the added hydrophobicity. Rather, we speculate that the backbone is significantly shielded from the aqueous environment by the side chains to reduce the enthalpic contribution of water-backbone interactions. Similarly, the 5 mol% carboxylic acid impurity along the backbone

is presumably not fully exposed to the aqueous environment and likely does not impact the CMC_a. Also, the effect of the alkane α-chain end impurity on micellization is assumed to be negligible because it represents less than 0.3wt% of the hydrophobic block and has a minimal difference in hydrophobicity compared to either the *tert*-butyl end group or the PPO repeat unit.

Analysis of the correlation functions via the second cumulant model (Eq. S1) shows that R_h increases approximately linearly with molecular weight, suggesting that the chains adopt an extended conformation in the micelles. Additionally, for every micellar BBP solution a biexponential model (Eq. S2), accounting for two relaxation rates, yields a superior fit than a single exponential model (Figs. S11–S13). Multi-angle DLS on a 3 mg/mL solution of the highest M_n polymer confirmed that both relaxation modes are diffusive and have R_h values larger than expected for a unimer, suggesting existence of a bimodal micelle size distribution (Fig. S14). The TEM micrograph in Fig. 4b also hints at a bimodal population of spherical micelles. This could be due to the direct dissolution method not allowing the micelle size distribution to fully equilibrate; however, the micelle size distribution does not change when annealed at 37 °C for 35 days (Fig. S15). This suggests the micelles have reached a steady state. Recent theoretical and experimental work has shown that the side chain length asymmetry of the two blocks can impact micelle morphology, aggregation number, and surface roughness due to packing frustration at the core-corona interface.[68–70,71] We hypothesize that the additional free energy contribution of side chain crowding near the core-corona interface creates at least two local minima in free energy-micelle size space that are separated by a significant energy barrier; thus leading to a bimodal micelle size distribution.

To estimate the micelle core radius (R_{core}), we modelled the core-forming block as a cylinder plus a hemisphere, where the cylinder length equals the contour length of the backbone and the hemisphere radius is twice the radius of gyration of a PPO side chain, Fig. S16. This simplified model assumes that the backbone is a rigid rod, the side chains are Gaussian coils, and that there is no chain overlap. Comparison of the calculated and experimental R_{core} values in Table 1 shows that this model is reasonable at short core block lengths ($N_{c,bb} \sim 5$), but is an overestimate for longer chains ($N_{c,bb} \sim 40$). This behavior resembles that of the Kratky-Porod wormlike chain model, and it suggests that in the micelle core a sufficiently long bottlebrush PPO can adopt a flexible conformation despite the high grafting density.[72,73] Finally, for polynorbornene grafted with 1 kDa PPO side chains a persistence length estimate of ~10 nm is consistent with a transition from rod-like to coil-like behavior occurring within the interval $5 < N_{c,bb} < 40$. This estimate is markedly higher than the 0.7 nm persistence length of a linear polynorbornene polymer,[74] as expected for a densely grafted bottlebrush.[31,75]

In conclusion, we report an efficient, high-throughput synthetic strategy to create bottlebrush poloxamers for the first time. The combination of living anionic and ROMP polymerization affords control over graft length and graft end-group and enables quantitative conversion of macromonomer. A series of hydrophilic bottlebrush poloxamers was synthesized over a range of molecular weights and the micellization behavior was compared to linear poloxamers. Bottlebrush poloxamers exhibit a remarkably reduced driving force for

micellization compared to linear poloxamers as evidenced by a two order of magnitude smaller scaling exponent between M_n and CMC_a.

Supplementary Material

Refer to Web version on PubMed Central for supplementary material.

Acknowledgements:

This work was supported by the National Institutes of Health (R01 HL122323 and R01 AR071349). NMR experiments reported in this publication was supported by the Office of the Director, National Institutes of Health, under Award Number S10OD011952. The content is solely the responsibility of the authors and does not necessarily represent the official views of the National Institutes of Health. The cryo-TEM images were taken using resources in the Characterization Facility, College of Science and Engineering, University of Minnesota, which receives partial support from the NSF through the MRSEC (Award Number DMR-2011401) and the NNCI (Award Number ECCS-2025124) programs. We also thank Dr. Michael Sims from the University of Minnesota for helpful discussions.

References:

(1). Wessels MG; Jayaraman A Molecular Dynamics Simulation Study of Linear, Bottlebrush, and Star-like Amphiphilic Block Polymer Assembly in Solution. Soft Matter 2019, 15 (19), 3987–3998. [PubMed: 31025695]

(2). Adams DJ; Kitchen C; Adams S; Furzeland S; Atkins D; Schuetz P; Fernyhough CM; Tzokova N; Ryan AJ; Butler MF On the Mechanism of Formation of Vesicles from Poly(Ethylene Oxide)-Block-Poly(Caprolactone) Copolymers. Soft Matter 2009, 5 (16), 3086–3096.

(3). Jiang Y; Lodge TP; Reineke TM Packaging PDNA by Polymeric ABC Micelles Simultaneously Achieves Colloidal Stability and Structural Control. J. Am. Chem. Soc. 2018, 140 (35), 11101–11111. [PubMed: 30137979]

(4). Maksym P; Neugebauer D Synthesis of Amphiphilic Semigrafted Pseudo-Pluronics for Self-Assemblies Carrying Indomethacin. RSC Adv. 2016, 6 (91), 88444–88452.

(5). Cotanda P; Lu A; Patterson JP; Petzetakis N; O'Reilly RK Functionalized Organocatalytic Nanoreactors: Hydrophobic Pockets for Acylation Reactions in Water. Macromolecules 2012, 45 (5), 2377–2384.

(6). Rabbel H; Werner M; Sommer JU Interactions of Amphiphilic Triblock Copolymers with Lipid Membranes: Modes of Interaction and Effect on Permeability Examined by Generic Monte Carlo Simulations. Macromolecules 2015, 48 (13), 4724–4732.

(7). De Mel JU; Gupta S; Willner L; Allgaier J; Stingaciu LR; Bleuel M; Schneider GJ Manipulating Phospholipid Vesicles at the Nanoscale: A Transformation from Unilamellar to Multilamellar by an n-Alkyl-Poly(Ethylene Oxide). Langmuir 2021, 37 (7), 2362–2375. [PubMed: 33570419]

(8). Adhikari U; Goliaei A; Tsereteli L; Berkowitz ML Properties of Poloxamer Molecules and Poloxamer Micelles Dissolved in Water and next to Lipid Bilayers: Results from Computer Simulations. J. Phys. Chem. B 2016, 120 (26), 5823–5830. [PubMed: 26719970]

(9). Redhead M; Mantovani G; Nawaz S; Carbone P; Gorecki DC; Alexander C; Bosquillon C Relationship between the Affinity of PEO-PPO-PEO Block Copolymers for Biological Membranes and Their Cellular Effects. Pharm. Res. 2012, 29 (7), 1908–1918. [PubMed: 22392332]

(10). Houang EM; Haman KJ; Kim M; Zhang W; Lowe DA; Sham YY; Lodge TP; Hackel BJ; Bates FS; Metzger JM Chemical End Group Modified Diblock Copolymers Elucidate Anchor and Chain Mechanism of Membrane Stabilization. Mol. Pharm. 2017, 14 (7), 2333–2339. [PubMed: 28538101]

(11). Kim M; Haman KJ; Houang EM; Zhang W; Yannopoulos D; Metzger JM; Bates FS; Hackel BJ PEO-PPO Diblock Copolymers Protect Myoblasts from Hypo-Osmotic Stress in Vitro Dependent on Copolymer Size, Composition, and Architecture. Biomacromolecules 2017, 18 (7), 2090–2101. [PubMed: 28535058]

(12). Zhang W; Haman KJ; Metzger JM; Hackel BJ; Bates FS; Lodge TP Quantifying Binding of Ethylene Oxide-Propylene Oxide Block Copolymers with Lipid Bilayers. Langmuir 2017, 33 (44), 12624–12634. [PubMed: 29068209]

(13). Lee RC; River LP; Pan FS; Ji L; Wollmann RL Surfactant-Induced Sealing of Electropermeabilized Skeletal Muscle Membranes in Vivo. Proc. Natl. Acad. Sci. U. S. A. 1992, 89 (10), 4524–4528. [PubMed: 1584787]

(14). Wang J-Y; Chen W; Nagao M; Shelat P; Hammer BAG; Tietjen GT; Cao KD; Henderson JM; He L; Lin B; Akgun B; Meron M; Qian S; Ward S; Marks JD; Emrick T; Lee KY C. Tailoring Biomimetic Phosphorylcholine-Containing Block Copolymers as Membrane-Targeting Cellular Rescue Agents. Biomacromolecules 2019, 20 (9), 3385–3391. [PubMed: 31424203]

(15). Terry MA; Hannig J; Carrillo CS; Beckett MA; Weichselbaum RR; Lee RC Oxidative Cell Membrane Alteration. Evidence for Surfactant-Mediated Sealing. Ann. N. Y. Acad. Sci. 1999, 888, 274–284. [PubMed: 10842639]

(16). Houang EM; Bartos J; Hackel BJ; Lodge TP; Yannopoulos D; Bates FS; Metzger JM Cardiac Muscle Membrane Stabilization in Myocardial Reperfusion Injury. JACC Basic to Transl. Sci. 2019, 4 (2), 275–287.

(17). Zhang W; Coughlin ML; Metzger JM; Hackel BJ; Bates FS; Lodge TP Influence of Cholesterol and Bilayer Curvature on the Interaction of PPO–PEO Block Copolymers with Liposomes. Langmuir 2019, 35 (22), 7231–7241. [PubMed: 31117745]

(18). Zhang W; Metzger JM; Hackel BJ; Bates FS; Lodge TP Influence of the Headgroup on the Interaction of Poly(Ethylene Oxide)-Poly(Propylene Oxide) Block Copolymers with Lipid Bilayers. J. Phys. Chem. B 2020, 124 (12), 2417–2424. [PubMed: 32175743]

(19). Firestone MA; Wolf AC; Seifert S Small-Angle X-Ray Scattering Study of the Interaction of Poly(Ethylene Oxide)-b-Poly(Propylene Oxide)-b-Poly(Ethylene Oxide) Triblock Copolymers with Lipid Bilayers. Biomacromolecules 2003, 4 (6), 1539–1549. [PubMed: 14606878]

(20). Firestone MA; Seifert S Interaction of Nonionic PEO-PPO Diblock Copolymers with Lipid Bilayers. Biomacromolecules 2005, 6 (5), 2678–2687. [PubMed: 16153106]

(21). Houang EM; Bates FS; Sham YY; Metzger JM All-Atom Molecular Dynamics-Based Analysis of Membrane-Stabilizing Copolymer Interactions with Lipid Bilayers Probed under Constant Surface Tensions. J. Phys. Chem. B 2017, 121 (47), 10657–10664. [PubMed: 29049887]

(22). Houang EM; Sham YY; Bates FS; Metzger JM Muscle Membrane Integrity in Duchenne Muscular Dystrophy: Recent Advances in Copolymer-Based Muscle Membrane Stabilizers. Skelet. Muscle 2018, 8 (1), 1–19. [PubMed: 29304851]

(23). Wang J; Segatori L; Biswal SL Probing the Association of Triblock Copolymers with Supported Lipid Membranes Using Microcantilevers. Soft Matter 2014, 10 (34), 6417–6424. [PubMed: 24978842]

(24). Kim M; Vala M; Ertsgaard CT; Oh S-H; Lodge TP; Bates FS; Hackel BJ Surface Plasmon Resonance Study of the Binding of PEO–PPO–PEO Triblock Copolymer and PEO Homopolymer to Supported Lipid Bilayers. Langmuir 2018, 34 (23), 6703–6712. [PubMed: 29787676]

(25). Kim M; Heinrich F; Haugstad G; Yu G; Yuan G; Satija SK; Zhang W; Seo HS; Metzger JM; Azarin SM; Lodge TP; Hackel BJ; Bates FS Spatial Distribution of PEO − PPO − PEO Block Copolymer and PEO 2 Homopolymer in Lipid Bilayers 1. 2020.

(26). Wu G; Majewski J; Ege C; Kjaer K; Weygand MJ; Lee KYC Lipid Corralling and Poloxamer Squeeze-out in Membranes. Phys. Rev. Lett. 2004, 93 (2), 2–5.

(27). Frey SL; Zhang D; Carignano MA; Szleifer I; Lee KYC Effects of Block Copolymer's Architecture on Its Association with Lipid Membranes: Experiments and Simulations. J. Chem. Phys. 2007, 127 (11).

(28). Cheng C; Wang J; Kausik R; Lee KYC; Han S Nature of Interactions between PEO-PPO-PEO Triblock Copolymers and Lipid Membranes: (II) Role of Hydration Dynamics Revealed by Dynamic Nuclear Polarization. Biomacromolecules 2012, 13, 2624–2633. [PubMed: 22808941]

(29). Wang J; Marks J; Lee KYC Nature of Interactions between PEO-PPO-PEO Triblock Copolymers and Lipid Membranes: (I) Effect of Polymer Hydrophobicity on Its Ability to Protect Liposomes from Peroxidation. Biomacromolecules 2012, 13, 2616–2623. [PubMed: 22808900]

(30). Togo T; Alderton JM; Bi GQ; Steinhardt RA The Mechanism of Facilitated Cell Membrane Resealing. J. Cell Sci. 1999, 112 (5), 719–731. [PubMed: 9973606]

(31). Lecommandoux S; Chécot F; Borsali R; Schappacher M; Deffieux A; Brûlet A; Cotton JP Effect of Dense Grafting on the Backbone Conformation of Bottlebrush Polymers: Determination of the Persistence Length in Solution. Macromolecules 2002, 35 (23), 8878–8881.

(32). Pietrasik J; Sumerlin BS; Lee H; Gil RR; Matyjaszewski K Structural Mobility of Molecular Bottle-Brushes Investigated by NMR Relaxation Dynamics. Polymer (Guildf). 2007, 48 (2), 496–501.

(33). Zhang B; Gröhn F; Pedersen JS; Fischer K; Schmidt M Conformation of Cylindrical Brushes in Solution: Effect of Side Chain Length. Macromolecules 2006, 39 (24), 8440–8450.

(34). Levi AE; Lequieu J; Horne JD; Bates MW; Ren JM; Delaney KT; Fredrickson GH; Bates CM Miktoarm Stars via Grafting-Through Copolymerization: Self-Assembly and the Star-to-Bottlebrush Transition. Macromolecules 2019, 52 (4), 1794–1802.

(35). López-Barrón CR; Brant P; Eberle APR; Crowther DJ Linear Rheology and Structure of Molecular Bottlebrushes with Short Side Chains. J. Rheol. (N. Y. N. Y). 2015, 59 (3), 865–883.

(36). Bichler KJ; Jakobi B; Schneider GJ Dynamical Comparison of Different Polymer Architectures - Bottlebrush vs Linear Polymer. Macromolecules 2021, 54 (4), 1829–1837. [PubMed: 33642616]

(37). Sun H; Yu DM; Shi S; Yuan Q; Fujinami S; Sun X Configurationally Constrained Crystallization of Brush Polymers with Poly(Ethylene Oxide) Side Chains. Macromolecules 2019, 52, 592–600.

(38). Chang AB; Bates FS Impact of Architectural Asymmetry on Frank-Kasper Phase Formation in Block Polymer Melts. ACS Nano 2020, 14, 11463–11472. [PubMed: 32820895]

(39). Shemper BS; Acar AE; Mathias LJ Synthesis of Linear and Starlike Polymers from Poly(Propylene Glycol) Methacrylate Using Controlled Radical Polymerization. J. Polym. Sci. Part A Polym. Chem. 2002, 40 (3), 334–343.

(40). París R; Quijada-Garrido I Synthesis and Aggregation Properties in Water Solution of Comblike Methacrylic Polymers with Oligo(Propylene Glycol)-Block-Oligo(Ethylene Glycol) as Side Chains. J. Polym. Sci. Part A Polym. Chem. 2011, 49 (8), 1928–1932.

(41). Truelsen JH; Kops J; Batsberg W; Armes SP Novel Polymeric Surfactants: Synthesis of Semi-Branched, Non-Ionic Triblock Copolymers Using ATRP. Macromol. Chem. Phys. 2002, 203 (14), 2124–2131.

(42). Maksym-Bębenek P; Biela T; Neugebauer D Water Soluble Well-Defined Acidic Graft Copolymers Based on a Poly(Propylene Glycol) Macromonomer. RSC Adv. 2015, 5 (5), 3627–3635.

(43). Loh XJ Poly(DMAEMA-Co-PPGMA): Dual-Responsive “Reversible” Micelles. J. Appl. Polym. Sci. 2013, 127 (2), 992–1000.

(44). Heroguez V; Gnanou Y; Fontanille M Novel Amphiphilic Architectures by Ring-Opening Metathesis Polymerization of Macromonomers. Macromolecules 1997, 30 (17).

(45). Heroguez V; Breunig S; Gnanou Y; Fontanille M Synthesis of α-Norbornenylpoly(Ethylene Oxide) Macromonomers and Their Ring-Opening Metathesis Polymerization. Macromolecules 1996, 29 (13).

(46). Ohnsorg ML; Prendergast PC; Robinson LL; Bockman MR; Bates FS; Reineke TM Bottlebrush Polymer Excipients Enhance Drug Solubility: Influence of End-Group Hydrophilicity and Thermoresponsiveness. ACS Macro Lett. 2021, 10 (3), 375–381. [PubMed: 35549060]

(47). Xia Y; Olsen BD; Kornfield JA; Grubbs RH Efficient Synthesis of Narrowly Dispersed Brush Copolymers and Study of Their Assemblies: The Importance of Side Chain Arrangement. J. Am. Chem. Soc. 2009, 131 (51), 18525–18532. [PubMed: 19947607]

(48). Hillmyer MA; Bates FS Synthesis and Characterization of Model Polyalkane - Poly (Ethylene Oxide) Block Copolymers. 1996, 9297 (96), 6994–7002.

(49). Ding J; Heatley F; Price C; Booth C Use of Crown Ether in the Anionic Polymerization of Propylene Oxide-2. Molecular Weight and Molecular Weight Distribution. Eur. Polym. J. 1991, 27 (9), 895–899.

(50). Heatley F; Lovell PA; Yamashita T Chain Transfer to Polymer in Free-Radical Solution Polymerization of 2-Ethylhexyl Acrylate Studied by NMR Spectroscopy. Macromolecules 2001, 34 (22), 7636–7641.

(51). Ding J; Heatley F; Price C; Booth C Use of Crown Ether in the Anionic Polymerization of Propylene Oxide-1. Rate of Polymerization. Eur. Polym. J. 1991, 27 (9), 891–895.

(52). Ren N; Zhu X Hybrid Polymerization of Ring-Opening Metathesis and Cross-Metathesis for Polyolefins with Tunable Architectures. Macromolecules 2018, 51 (23), 9555–9561.

(53). Zhang H; Zhang Z; Gnanou Y; Hadjichristidis N Well-Defined Polyethylene-Based Random, Block, and Bilayered Molecular Cobrushes. Macromolecules 2015, 48 (11), 3556–3562.

(54). Yavitt BM; Fei H; Kopanati G; Li R; Fukuto M; Winter HH; Watkins JJ Long-Range Lamellar Alignment in Diblock Bottlebrush Copolymers via Controlled Oscillatory Shear. Macromolecules 2020.

(55). Schillén K; Brown W; Johnsen RM Micellar Sphere-to-Rod Transition in an Aqueous Triblock Copolymer System. A Dynamic Light Scattering Study of Translational and Rotational Diffusion. Macromolecules 1994, 27 (17), 4825–4832.

(56). Early JT; Lodge TP Fragmentation of 1,2-Polybutadiene- Block-Poly(Ethylene Oxide) Micelles in Imidazolium-Based Ionic Liquids. Macromolecules 2019, 52 (18), 7089–7101.

(57). Zee N. J. Van; Hillmyer MA; Lodge TP. Role of Polymer Excipients in the Kinetic Stabilization of Drug-Rich Nanoparticles. ACS Appl. Bio Mater. 2020, 3, 7243–7254.

(58). Kangarlou B; Dahanayake R; Martin IJ; Ndaya D; Wu C-M; Kasi RM; Dormidontova EE; Nieh M-P Flower-like Micelles of Polyethylene Oxide End-Capped with Cholesterol. Macromolecules 2021, 54 (19), 8960–8970.

(59). Alexandridis P; Holzwarth JF; Hatton TA Micellization of Poly(Ethylene Oxide)-Poly(Propylene Oxide)-Poly(Ethylene Oxide) Triblock Copolymers in Aqueous Solutions: Thermodynamics of Copolymer Association. Macromolecules 1994, 27 (9), 2414–2425.

(60). Yang YW; Deng NJ; Yu GE; Zhou ZK; Attwood D; Booth C Micellization of Diblock and Triblock Copolymers in Aqueous Solution. New Results for Oxyethylene/Oxybutylene Copolymers E38B12 and E21B11E21. Comparison of Oxyethylene/Oxybutylene, Oxyethylene/ Oxypropylene, and Oxyethylene/Alkyl Systems. Langmuir 1995, 11 (12), 4703–4711.

(61). Topel Ö; Çakir BA; Budama L; Hoda N Determination of Critical Micelle Concentration of Polybutadiene-Block-Poly(Ethyleneoxide) Diblock Copolymer by Fluorescence Spectroscopy and Dynamic Light Scattering. J. Mol. Liq. 2013, 177, 40–43.

(62). Alexandridis P; Hatton TA Block Copolymer Surfactants in Aqueous Solutions and at Interface: Thermodynamics, Structure, Dynamics and Modeling. Colloids Surfaces A Physicochem. Eng. Asp. 1995, 96, 1–46.

(63). Nyrkova IA; Semenov AN On the Theory of Micellization Kinetics. Macromol. Theory Simulations 2005, 14 (9), 569–585.

(64). Tuzar Z; Štěpánek P; Koňák Č; Kratochvíl P Block Copolymer Micelles near Critical Conditions. J. Colloid Interface Sci. 1985, 105 (2), 372–377.

(65). Leibler L; Orland H; Wheeler JC Theory of Critical Micelle Concentration for Solutions of Block Copolymers. J. Chem. Phys. 1983, 79 (7), 3550–3557.

(66). Much MR; Gast AP Block Copolymers at Interfaces. 1. Micelle Formation. Macromolecules 1988, 21 (18), 1360–1366.

(67). Lyubimov I; Wessels MG; Jayaraman A Molecular Dynamics Simulation and PRISM Theory Study of Assembly in Solutions of Amphiphilic Bottlebrush Block Copolymers. Macromolecules 2018, 51 (19), 7586–7599.

(68). Zhulina EB; Borisov OV Micelles Formed by an AB Copolymer with Bottlebrush Blocks: Scaling Theory. J. Phys. Chem. B 2021.

(69). Grundler J; Shin K; Suh H-W; Zhong M; Saltzman WM Surface Topography of Polyethylene Glycol Shell Nanoparticles Formed from Bottlebrush Block Copolymers Controls Interactions with Proteins and Cells. ACS Nano 2021, 15 (10), 16118–16129. [PubMed: 34633171]

(70). Fenyves R; Schmutz M; Horner IJ; Bright FV; Rzayev J Aqueous Self-Assembly of Giant Bottlebrush Block Copolymer Surfactants as Shape-Tunable Building Blocks. J. Am. Chem. Soc. 2014, 136 (21), 7762–7770. [PubMed: 24819562]

(71). Alaboalirat M; Qi L; Arrington KJ; Qian S; Keum JK; Mei H; Littrell KC; Sumpter BG; Carrillo JMY; Verduzco R; Matson JB Amphiphilic Bottlebrush Block Copolymers: Analysis of

Aqueous Self-Assembly by Small-Angle Neutron Scattering and Surface Tension Measurements. Macromolecules 2019, 52 (2), 465–476.

(72). Kratky O; Porod G Rontgenuntersuchung Geloster Fadenmolekule. Rec. Trav. Chim. 1949, 68, 1106–1122.

(73). Sunday DF; Chremos A; Martin TB; Chang AB; Burns AB; Grubbs RH Concentration Dependence of the Size and Symmetry of a Bottlebrush Polymer in a Good Solvent. Macromolecules 2020, 53 (16), 7132–7140. [PubMed: 34121772]

(74). Liu C; Kubo K; Wang E; Han KS; Yang F; Chen G; Escobedo FA; Coates GW; Chen P Single Polymer Growth Dynamics. Science (80-.) 2017, 358 (6361), 352–355.

(75). Haugan IN; Maher MJ; Chang AB; Lin TP; Grubbs RH; Hillmyer MA; Bates FS Consequences of Grafting Density on the Linear Viscoelastic Behavior of Graft Polymers. ACS Macro Lett. 2018, 7 (5), 525–530. [PubMed: 35632925]

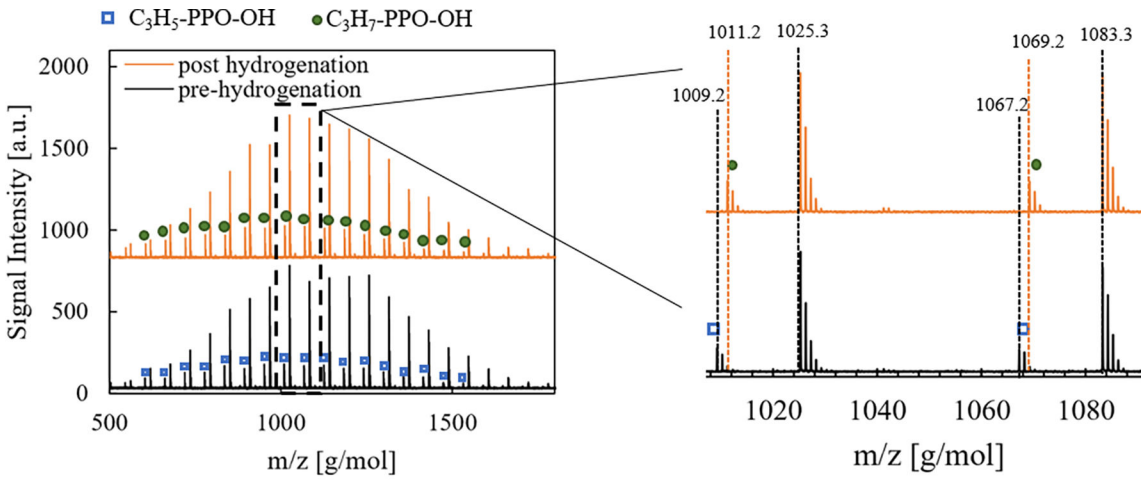

Figure 1.

MALDI-ToF data of PPO polymer as synthesized via anionic polymerization (black) and post hydrogenation (orange). M_w = 1220 g/mol and $Đ$ = 1.12 for both polymers. The most intense family of peaks in both samples is *tert*-butyl-PPO-OH (*t*-PPO-OH) and is unchanged during hydrogenation. Alkene and alkane α-chain end impurities are labelled accordingly.

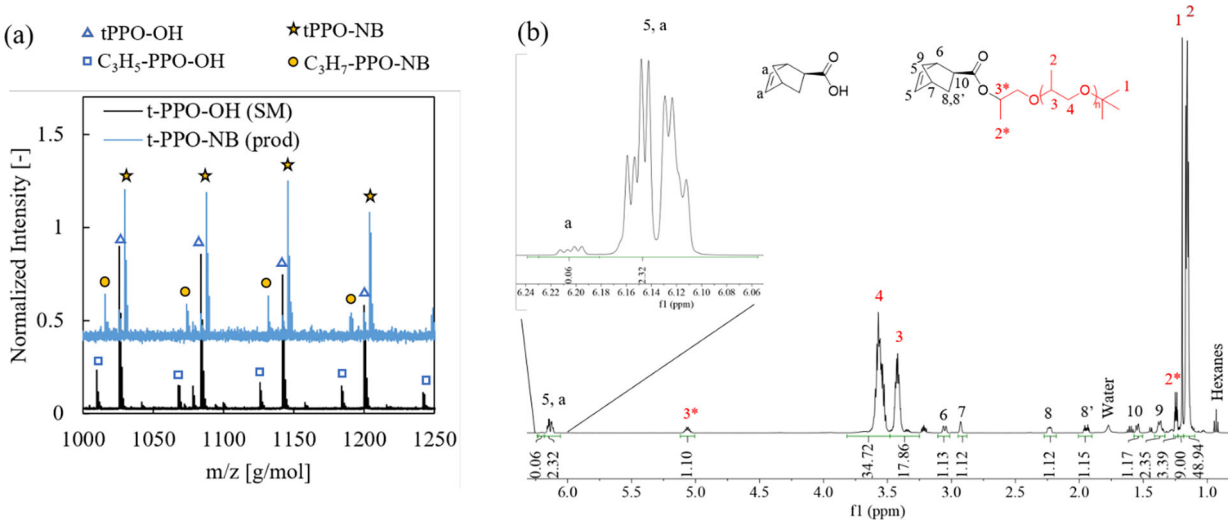

Figure 2.

(a) MALDI of *t*-PPO-OH and the NB functionalized macromonomer, *t*-PPO-NB, following the hydrogenation and esterification reactions. M_w = 1210 g/mol and $Đ$ = 1.12 for the SM and M_w = 1330 g/mol and $Đ$ = 1.14 for the product. (b) ^{1}H NMR spectrum of the *t*-PPO-NB macromonomer.

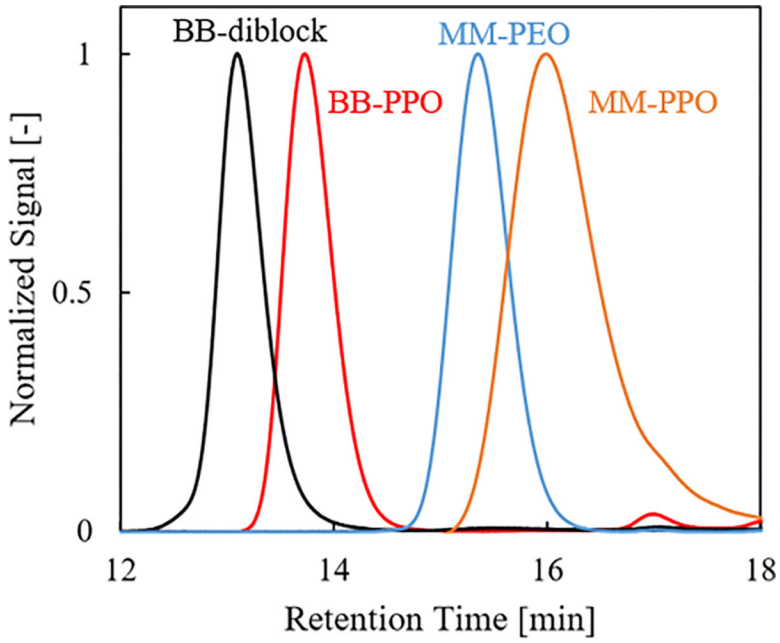

Figure 3.

SEC traces with differential refractive index detection of a representative sequential ROMP polymer (BB-$E_{45,\ 20}$-*b*-BB-$P_{15,\ 10}$). The macromonomer traces are included for reference. From the multi-angle light scattering detector and a Zimm analysis, the BB-PPO aliquot has a M_w = 11,600 g/mol and $Đ$ = 1.20 and the BB-diblock has a M_w = 55,300 g/mol and Đ = 1.10, both were within error of the targeted molecular weight. The small peak at ~17 minutes in the BB-PPO chromatogram is likely a small molecule impurity in the PPO macromonomer, possibly 18-crown-6 ether, that does not impact the subsequent polymerization

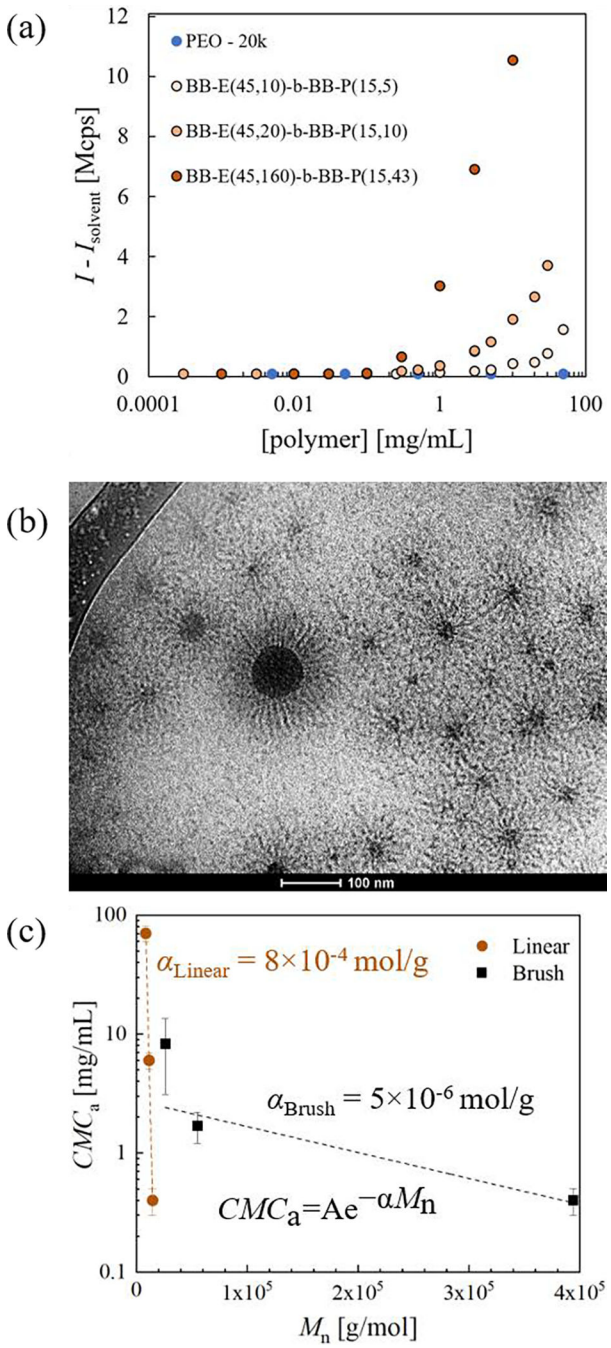

Figure 4.

(a) Excess scattering intensity at 37 °C, as a function of polymer concentration. Linear PEO with an M_n = 20 kDa is a negative control for micellization. (b) cryo-TEM micrograph of BB-E(45,160)-b-BB-P(15,43) at a concentration of 10 mg/mL in aqueous buffer with 40,000x magnification. (c) Trend between CMC_a and M_n for linear and bottlebrush poloxamers of similar wt% PEO. Data for linear poloxamers (40 °C) is taken from Alexandridis et al.[59] Data are fit to the exponential function shown on the graph and the correlation coefficients are 0.99 and 0.58 for linear and brush, respectively.

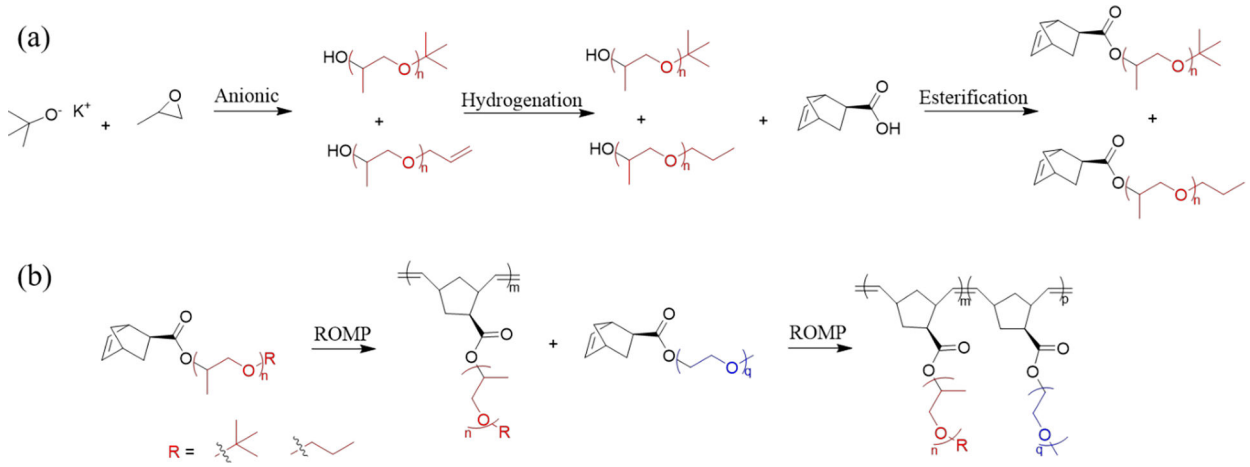

Scheme 1:

Reaction scheme to synthesize bottlebrush poloxamers

(a) Anionic polymerization was initiated with potassium *tert*-butoxide and ran to full conversion at 40 °C in the presence of 18-crown-6 ether. Hydrogenation was achieved over palladium on carbon. Esterification used a 50% molar excess of norbornene-carboxylic acid and was facilitated by DIC and DMAP. (b) Sequential ROMP was performed using Grubbs 3rd generation catalyst.

Table 1:

Materials and micellization data summary.

Polymer	M_n [g/mol][a]	$Đ$ [a]	wt% PEO[a]	wt% NB[a]	*CMC*a [mg/mL][b]	R_h [nm][c]	R_{core} [nm][d] (calc)	R_{core} [nm][e] (expt)
E_{450} (PEO-20k)	20000	1.10	100	0	N/A			
E_{76}-*b*-P_{29}-*b*-E_{76} (F68)[f]	8400[f]		80[f]	0	70 ± 10[f]			
E_{103}-*b*-P_{39}-*b*-E_{103} (F88)[f]	11400[f]		80[f]	0	6 ± 0.9[f]			
E_{132}-*b*-P_{50}-*b*-E_{132} (F108)[f]	14600[f]		80[f]	0	0.4 ± 0.1[f]			
BB-$E_{45,10}$-*b*-BB-$P_{15,5}$	26200	1.07	72	8	8 ± 3	17 ± 4	5	6 ± 1
BB-$E_{45,20}$-*b*-BB-$P_{15,10}$	55000	1.10	74	8	2 ± 0.5	25	8	
BB-$E_{45,160}$-*b*-BB-$P_{15,43}$	394000	1.15	80	7	0.4 ± 0.1	150	30	15 ± 8

[a] SEC with multi-angle light scattering detection and Zimm analysis

[b] Determined by DLS

[c] DLS data reported for 10 mg/mL solution using the second cumulant model. Error is the standard deviation of three independent replicates.

[d] Model described in Fig. S16: sum of core forming block's backbone contour length and twice the radius of gyration of its side chains

[e] Determined by cryo-TEM

[f] Data from Alexandridis et al. *Macromolecules*. 1994, 27, 9, 2414–2425 measured via fluorescent dye method.[59]